Journal of Earthquake & Tsunami

Impulsive waves generated by the collapse of a submerged granular column: a three-phase flow simulation with an emphasis on the effects of initial packing condition

Ming-Lan Yu, Cheng-Hsien Lee*

Department of Water Resources and Environmental Engineering, Tamkang University, Taiwan

Zhenhua Huang

Department of Ocean and Resources Engineering, School of Ocean and Earth Science and Technology, University of Hawaii at Manoa, Honolulu HI 96822, USA

Received date
Accepted date

Submarine landslides are one of the major causes of tsunamis but less understood due to complicated dynamics involved and the lack of observational data. In this study, the collapse of a submerged granular column is used as an idealized submarine landslide model. A three-phase (solid-water-gas) continuum model is used to study the effect of the column's initial packing on the collapse process and the resultant waves. Numerical simulations reveal that the initial packing can have significant effect on the duration of the collapse process and the characteristics of the resultant waves. Pore pressure, velocity field of the fluid phase, the volume of the sliding granular mass, and the sliding velocity are calculated and used to understand the effects of initial packing condition. Our results show that it is important to consider the initial packing effects in numerical simulations of submarine landslides and the resultant waves. Our result also show that the large vortex generated by the moving front of the granular flow can affect the the form of the waves generated by the landslide.

Keywords: Submarine landslide; Tsunami; Solid-liquid-gas flow; Multiphase flow; Large vortex; Kelvin-Helmholtz instability; Pore pressure

1. Introduction

In addition to submarine earthquakes, submarine landslides are another major cause of tsunamis. Generally speaking, the landslide volume determines the tsunamigenic strength [Løvholt et al., 2015], but there exist exceptions; for example, the giant Tænadjupet slide, occurring at the edge of Norway's continental shelf in 4500 BP, did not generate destructive tsunamis due to unknown complicated dynamics [Løvholt et al., 2017]. Due to the extreme long scales of tsunami waves, it is difficult to simulate the tsunamis in laboratory without introducing scale distortion. Numerical models, after careful calibration using small-scale test results, can provide another

*Corresponding author. Email address: kethenlee@gmail.com

tool to investigate the relationship between the landslide dynamics and the resulting waves, and has the potential to perform large-scale simulation of tsunami generation without scale distortion.

Landslide tsunamis have been widely studied experimentally and numerically using solid block models [Enet and Grilli, 2007; Fritz et al., 2003; Heinrich, 1992; Hill et al., 2014; Liu et al., 2005]. These models, however, cannot study the effects of the changing volume and shape of the sliding mass. These shortcomings can be avoided by modeling the landslide as a collapse process of submerged granular material in laboratory or through solid-liquid two-phase flow modeling. To understand the fundamentals of the dynamics involved in submarine landslides through a granular flow approach, the collapse of a granular column submerged in a fluid has been frequently used as a simple model of submarine landslides in previous studies [Meruane et al., 2010; Meruane et al., 2012; Rondon et al., 2011; Topin et al., 2012]. Unlike the collapse of a dry granular column, a submerged column of the same dimension, composition and properties has been found to have a slower spreading velocity than the corresponding dry granular column [Meruane et al., 2010], which is due mainly to the increased drag between the granular material and the surrounding fluid. It has also been found in previous studies that the initial packing can significantly affect the collapse process [Rondon et al., 2011]: a granular column with an initially-dense packing has a collapse duration longer than a granular column with the same conditions but an initially-loose packing. Topin et al. [2012] performed two-dimensional discrete-element simulations of collapsing granular columns in different fluids; they found that the ambient fluid can dissipate the kinetic energy of the solid grains and enhance the spreading by lubrication between grains and that the submerged collapse may have longer or shorter runout distance than the collapse in air, depending on fluid's viscosity. Several experimental studies on the waves generated by submarine granular slides [Assier Rzadkiewicz et al., 1997; Grilli et al., 2017] can be found in literature; these studies focus on submarine granular slides down inclined planes with steep slopes. The measured free-surface displacement was provided mainly for comparisons with the results computed by numerical models.

Several numerical models have been developed to study the waves generated by submarine landslides. However, these models normally treat the landslides and the hydrodynamics separately. To simulate the hydrodynamics, one group of models solve depth-resolving equations, such as Navier-Stokes equations [Abadie et al., 2012; Gauer et al., 2005; Horrillo et al., 2013; Hill et al. 2014; Ma et al., 2015; Shi et al., 2016]. Since resolving flow variation in depth requires huge computational resources, the other group of models solve depth-averaged equations such as shallow-water equations instead [Løvholt et al., 2017; Yavari-Ramshe and Ataie-Ashtiani, 2016]. To simulate submarine landslides, several approaches have been used in the past. The simplest approach is to consider the landslide as a rigid block whose motion is specified by empirical equations derived from either laboratory measurements

[Hill et al., 2014] or the balance of various forces acting on the sliding block [Enet and Griiil, 2007]. To account for the deformation of the sliding volume, one group of models solves one-layer depth averaged equations, such as the Savage-Hutter model, to describe the motion and deformation of the sliding volume [Løvholt et al., 2017; Ma et al., 2015; Si et al, 2017; Yavari-Ramshe and Ataie-Ashtiani, 2016], and the other group of numerical models treats the released the granular mass as either Newtonian fluid [Abadie et al., 2012, Horrillo et al., 2013] or Non-Newtonian fluid [Gauer et al., 2005]. Recently, elastoplastic models have also been applied to study the submarine landslides [Shi et al., 2016].

All these aforementioned models consider landslides as a single-phase motion and the relative motion between solid grains and the surrounding water in the sliding granular mass has been ignored. We are not aware of applications of three-phase flow models to study waves generated by submarine landslides. We report in this study an attempt of applying a solid-liquid-gas three phase model to investigate the waves generated by the collapse of a submerged granular columns, with a focus on the column's initial packing.

2. Mathematical formulas

The three-phase model used in this study treats the granular materials as an continuum solid phase and treats the liquid and gas as a single fluid phase of water-air mixture with a variable density and a variable viscosity. In other word, the three-phase model is implemented as a semi-two phase flow model. The air-water interface is tracked by a Volume-of-Fluid (VOF) method, which be implemented in the presence of suspended sediment [Lee, et al., 2018] . The constitutive laws, which are used to model the pressures and stresses in fluid and solid phases and to model the forces between the solid and the fluid phases, are different among different two/three phase flow models. The constitutive laws used in this study have been successfully applied to simulate the collapse of granular column submerged in a fluid without a free surface [Lee and Huang, 2018] and waves generated by subaerial landslides which involves water, air and solid phases [Lee and Huang, 2017].

For completeness, the key equations and constitutive laws are summarized below. The reader is referred to Lee and Huang[2018] and Lee et al. [2018] for details. The air-water mixture is described by the so-called liquid saturation, s, which classifies whether a spatial point is occupied by air ($s = 0$), water ($s = 1$), or both ($0 < s < 1$). The same method has been used in the VOF method for air-water surface tracking [Hirt, 1981]. The density, ρ_f, and viscosity, ν_f, of the air-water mixture are computed by

$$\rho_f = s\rho_w + (1 - s)\rho_a, \tag{1}$$

and

$$\nu_f = s\nu_w + (1 - s)\nu_a, \tag{2}$$

where ρ_w and ρ_a are the densities of the water and air phases, respectively; ν_w and ν_a are the kinematic viscosities of the water and air phases, respectively. The relative velocities between the water and air phases are assumed to be zero everywhere.

The following three equations govern the conservation of mass for the solid, water and air phases, respectively:

$$\frac{\partial c}{\partial t} + \nabla \cdot [c\mathbf{u}^s] = 0, \tag{3}$$

$$\frac{\partial s}{\partial t} + \nabla \cdot \left[s\mathbf{u}^f\right] - s\nabla \cdot \mathbf{u}^f = 0, \tag{4}$$

and

$$\nabla \cdot [(1-c)\mathbf{u}^f + c\mathbf{u}^s] = 0, \tag{5}$$

where c is the volume of concentration for the sediment phase; $\mathbf{u}$ is the velocity. The superscript or subscript s and f refer to the solid and fluid phases, respectively. Eq. (3) and Eq. (4) are used to determine c and s, and Eq. (5) reflects the incompressibility of both the fluid and sediment phases, and is used to correct the fluid-phase pressure, p_f.

The equations governing the conservation of momentum are listed below:

$$\begin{aligned}\frac{\partial \rho_s c\mathbf{u}^s}{\partial t} + \nabla \cdot [\rho_s c\mathbf{u}^s\mathbf{u}^s] =& \rho_s cg - c\nabla p_f - \nabla(cp_s) + \nabla \cdot [c\mathbf{T}^s] \\ &+ c\rho_s \frac{(\mathbf{u}^f - \mathbf{u}^s)}{\tau_p} - \frac{\rho_s}{\tau_p}\frac{(1-c)\nu_{ft}}{\sigma_c}\nabla c\end{aligned} \tag{6}$$

for the sediment phase, and

$$\begin{aligned}\frac{\partial \rho_f (1-c)\mathbf{u}^f}{\partial t} + \nabla \cdot [\rho_f (1-c)\mathbf{u}^f\mathbf{u}^f] =& \rho_f (1-c)g - (1-c)\nabla p_f + \nabla \cdot \left[(1-c)\mathbf{T}^f\right] \\ &- c\rho_s \frac{\mathbf{u}^f - \mathbf{u}^s}{\tau_p} + \frac{\rho_s}{\tau_p}\frac{(1-c)\nu_{ft}}{\sigma_c}\nabla c\end{aligned} \tag{7}$$

for the fluid phase. In Eqs. (6) and (7), ρ is the density; c is the volume concentration of sediment; $\mathbf{g}$ is the gravitational acceleration; p is the pressure; $\mathbf{T}$ is the stress tensor; τ_p is the particle response time; ν_{ft} is the eddy viscosity of the fluid phase; σ_c is the Schmidt number. The momentum exchange between the solid and fluid phases are accounted for by the last two terms in Eqs. (6) and (7): the first term accounts for the drag force and the second term for turbulent dispersion.

Constitutive models for $\mathbf{T}^f$, ν_{ft}, $\mathbf{T}^s$, p_s, and τ_p are required in order to solve Eqs. (6) - (7). The three-phase model of Lee et al. [2018] adopts the $k-\epsilon$ model with a low-Reynolds-number correction to compute $\mathbf{T}_f$ and ν_{ft} [Lee et al., 2016]. In addition to the turbulent motion of solid phase in low concentration [Hinze, 1972] and elastic effect in high concentration [Hsu et al., 2004], the visco-plastic rheological characteristics and the dilatancy behavior [Forterre and Pouliquen, 2008] are considered in computing $\mathbf{T}^s$ and p_s, respectively. For dense flows, both the visco-plastic rheological characteristics and the concentration highly depend on a

combined dimensionless parameter, $I = I_v + aI_i^2$, where I_v is the viscous number, I_i is the inertial number, and a is a constant [Trulsson et al., 2012]. The viscous number describes the ratio of the viscous stress to the quasi-static shear stress associated with the weight (due to the enduring contact), and it is defined by $I_v = 2\rho_f \nu_f D^s / cp_s$ where ν_f = the kinematic viscosity of the fluid, D^s = the second invariant of the strain rate, and d = the particle diameter. The inertial number, defined by $I_i = 2dD^s/\sqrt{cp_s/\rho_s}$, describes the ratio of the inertial stress to the quasi-static stress. Some formulas have been proposed to describe $c - I$ and $\eta - I$ relationships, where $\eta = T^s/p_s$ with T^s being the second invariant of $\mathbf{T}^s$. In the model of Lee et al. [2018], the following two formulas have been used:

$$\eta = \eta_1 + \frac{\eta_2 - \eta_1}{1 + I_o/I}, \tag{8}$$

where η_2 and I_o are constants and $\eta_1 = \tan\theta_s$ with θ_s = the angle of repose, and

$$c = \frac{c_c}{1 + bI^{1/2}}, \tag{9}$$

where c_c is a critical concentration representing the maximum packing fraction of an homogeneously sheared assembly of frictional spheres [Boyer et al., 2011] and b is a model parameter. The particle response time is computed by the formula suggested by Lee and Huang [2018], which is a combination of the formula of Richardson and Zaki [1954] for low concentration and that of Engelund [1953] for high concentration. The former was obtained from sedimentation experiments and the later from experiments of steady uniform flow through porous media.

In summary, the present model is based on the rheological characteristics of the solid phase, which is proposed for high concentration flows. The model considers the turbulent motions for the solid and fluid (liquid and gas) phases, which are significant for low concentration flows. The model we used to compute the drag force is applicable from low to high concentration flows.We remark that Wang et al. [2017] recently developed a two-phase model that can be also used to study landslide-induced waves. The model of Wang et al. [2017] considers the granular material as an elastic-perfectly plastic material but does not take the turbulence effect into account; the method they used to compute the drag force is applicable only to high concentration flows. Although Wang et al. [2017] used a sophisticated approach to deal with the solid phase, the present model is applicable to flows with a wide range of solid-phase concentrations.

3. Numerical setups

The three-phase flow model [Lee et al., 2018] was developed using OpenFOAM (foam-extend-4.0). OpenFOAM is a free, open-source computational fluid dynamics (CFD) toolbox [Jasak, 2009]. The numerical stability can be improved by incorporating a perdition-correction scheme proposed by Lee et al. [2015] into the

"PIMPLE" scheme, which changes the discrete mass-balance equation for the sediment phase to an advection-diffusion equation instead of an advection equation. The diffusion behavior of the numerical scheme helps subdue the fluctuation in concentration, and thus increases the numerical stability which might occur at high concentration.

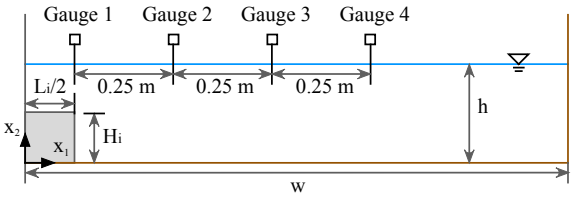

Fig. 1. Numerical setup. Only half of the column in shown here due to the geometric symmetry of the problem about $x_1 = 0$.

The model is applied to simulate the collapse of a submerged granular column and the resultant waves shown in Fig. 1, where the positive direction of x_1 axis points to the right, H_i is the initial height of the column, L_i is the initial length, h is the initial water depth, and w is the length of the computational domain. $w = 4$ m is taken here. The column is symmetric about x_1 =0, therefore only half of the column in the region of $x > 0$ needs to be simulated in the numerical experiment. Due to the geometric symmetry, the vertical plane of $x_1 = 0$ is treated as a smooth rigid wall in the simulation, and all numerical simulations are performed only for one half of the column in the region of $x_1 > 0$. Initially, a force is applied on the granular column to keep it in its static state and that force is removed instantaneously at $t = 0$ s to initiate the landslide. The numerical results will be presented only for the half of the column in the region of $x_1 > 0$ due to the geometric symmetry.

The dimensions and properties of the columns examined in this study are listed in Table 1, including water depth h, initial height of the column H_i, initial length of the column L_i, the column aspect ration $R = H_i/L_i$, the initial concentration c_i, and the grian diameter d. To understand the effect of the column's initial packing on the resultant waves, two initial packing conditions are examined: $c_i = 0.553$ for initially-loose packing condition and $c_i = 0.558$ for initially-dense packing condition. Because the focus of this study is on the effect of initial packing, only the results for the particle size $d = 0.5$ mm and a height-width ratio $R = 0.5$ are discussed in the rest of the paper.

Table 1. Dimensions and properties of the submerged granular columns.

Case	$L_i(cm)$	$H_i(cm)$	$R = H_i/L_i$	$h(cm)$	c_i	d (mm)
1	46	23	0.5	25	0.553	0.5
2	46	23	0.5	25	0.58	0.5

Similar to previous numerical studies of collapses of dry granular columns on a rough bed [Lee et al., 2015] and submerged granular columns on a rough bed [Lee and Huang, 2018], the no-slip boundary condition is imposed at the bed but a slip boundary condition is implemented at $x = 0$ for the solid phase. For the fluid phase, the wall-function method is imposed at the bed and at two lateral walls. Most of the parameters used in this study are the same as those in the previous study of Lee and Huang [2018], except for a_E and b_E used in computing the particle response time; these two parameters (which determines the permeability for packed sediment) depend on the sediment composition and arrangements. $a_E = 760$ and $b_E = 1.5$ are used in this study for uniform sphere particles with a random packing condition.

4. Results and discussion

The validation and verification of the solid-water-gas three-phase model and our code have been reported elsewhere, including: (1) Lee and Huang [2018], who used the model to reproduce the experimental results of Rondon et al. [2011] on the collapse of a granular column in a liquid for two packing conditions, (2) Lee et al. [2018], who used the model to reproduce the experiment of Chatterjee, et al. [1994] on the local scour induced by a submerged wall jet, and (3) Lee and Huang [2017], who used the model to reproduce the experimental results of Viroulet et al. [2013] on the impulsive waves generated by a subaerial landslide.

4.1. *Description of collapse process and resultant waves*

Fig. 2 shows the simulated collapse process and the resultant waves for the granular column with an initially-loose packing condition (Case 1). In the early stage of the collapse ($t < 0.2$ s), the top of the column drops and the front face moves forward. From $t = 0.2$ s to $t = 1.6$ s the interface between the water and the granular mass continues to flatten out; the granular flow front continues to move froward and eventually stops when $t > 1.6$ s. The motion of the granular mass generates surface waves. At $t = 0.2$ s, two waves can be identified: a right-going positive wave (marked by the letter A in the figure) and a surface depression or wave trough (marked by the letter B in the figure). At $t = 0.4$ s there is a hump on the air-water interface from $x_1 \approx 10$ cm (marked by point D) to $x_1 \approx 17$ cm (marked by point C). It will be shown later in the discussion of the flow field that the vortex motion generated by the granular flow front is responsible for the presence of this hump. The surface disturbance due to this hump propagates as a secondary wave to the left and collide at $x_1 = 0$ cm with the same secondary wave coming from the left (due to the geometric symmetry), resulting in a large surface elevation at $x_1 = 0$ cm at $t = 0.6$ s. After colliding, the the secondary wave coming from the left continues to propagate to the right at $t = 0.8$ s, and gradually merges with the right tail of the secondary wave going to the right at $t = 1.2$ s.

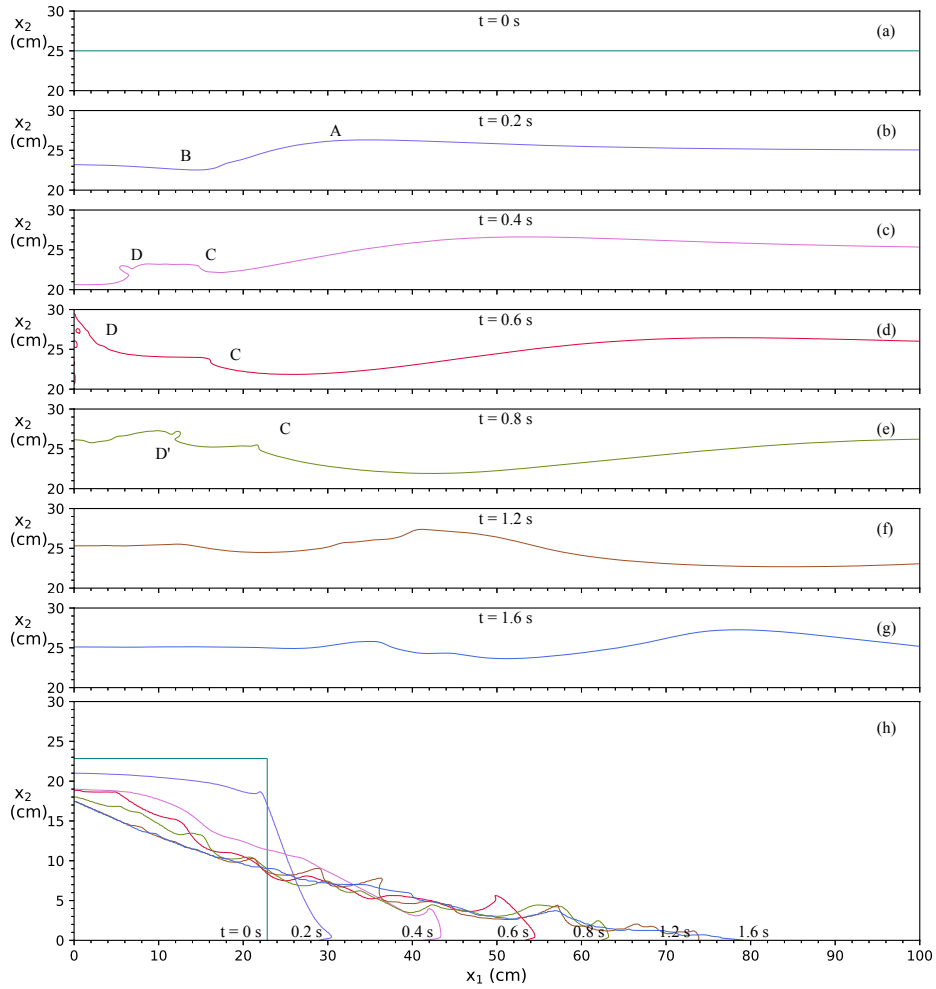

Fig. 2. The simulated profiles of the water surface ($s = 0.5$) [(a)-(g)] and the interfaces between the water and the granular mass (h) at $t = 0$ s (a), 0.2 s (b), 0.4 s (c), 0.6 s (d), 0.8 s (e), 1.2 s (f), and 1.6 s (g) for Case 1.

Fig. 3 shows the collapse process and the resultant waves for the granular column with an initially-dense packing condition (Case 2). Compared to Fig. 2, the granular column with an initially-dense packing condition has a slower collapse process and the resultant waves are slightly weaker. Because the initial packing condition affects the speed of the collapse and the resulting waves, it is important to consider it in the numerical simulations of landslide-induced waves.

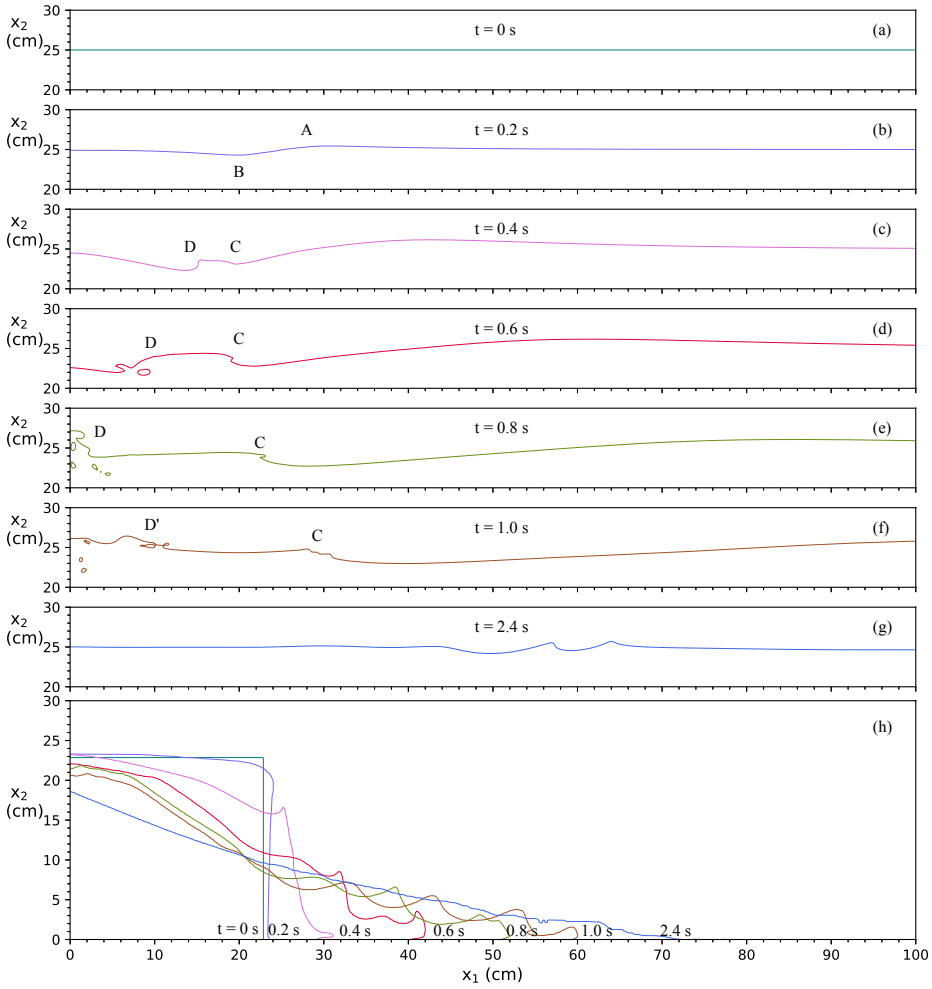

Fig. 3. Snapshots of the simulated collapse process and surface profile for Case 2.

4.2. *Flow field*

Three snapshots of the flow field generated by the collapse of the column are presented in Fig. 4 for the initially-loose packing condition (Case 1) and Fig. 5 for the initially-dense packing condition (Case 2). A solid line below the interface between the water and the granular mass is used to indicate the failure line at the instant of the snapshot. This failure line is determined using the the isovelocity line for the magnitude of the solid-phase velocity being 5 cm/s. The arrows in these figures indicate the velocity of the fluid phase, and the color in the background represents the volume concentration of the solid phase.

For the initially-loose packing case (Fig. 4), the snapshot for $t = 0.4$ s shows

that a large volume of granular mass slides down along a surface defined by the failure line, below which the grains are practically not moveing. It can be seen that the volume of granular mass reduces with the elapse of time. The motion of the granular flow front generates a large vortex (scaled by the depth of the water), which can leave a signature of its existence on the free surface. In particular, the strong vortex motion causes the water near the surface to flow towards left, producing the hump found on the water surface between $x \approx 10$ cm and $x \approx 17$ cm (see also the description and discussion of Fig. 2 in Section 4.1). This vortex motion can penetrate deep into the granular mass, affecting in turn the speed of the granular flow front. At $t = 0.8$ s, the failure line is getting closer to the interface between the water and the granular mass, indicating that the volume of granular mass in motion is reduced compared to that at $t = 0.2$ s; both the strength and the size of the vortex are reduced, too. At $t = 1.2$ s, the sliding process is about to stop, as indicated by the volume of the granular mass in motion; the vortex motion becomes insignificant except for some near-periodic small-scale vortexes generated probably by shear-induced instability (Kelvin-Helmholtz instability [White, 2000]). We remark that these small vortexes may be responsible for maintaining some granular materials in suspension close to the interface between the water and the granular material.

For the initially-dense packing case (Fig. 5), the duration of the collapse process is longer, which means the speed of the granular flow front is slower compared to the initially-loose packing condition. Similar phenomena found in the loose packing column can also be found here, such as large vortex close to the flow front in early stage of the collapse and the near-periodic small-scale vortexes in the later stage of the collapse. Even though the existence of the vortex motion generated by the granular flow front still shows itself through a hump on the water surface, the size of the hump is much smaller.

The experimental results of Wang et al. [2017] suggest that in higher fluid-viscosity condition, the initial packing has more significant effect on runout. Figs. 4 and 5 show similar runout for the initially-loose and initially-dense packing cases; this is because the viscosity of water is much smaller than that used in the experiment of Rondon et al [2011]. Rondon et al. [2011] used a mixture of water and oil, which has a dynamic viscosity 12 times higher than that of water, and found that the runout distance of an initially-dense packing column is much less than that of that of an initially-loose packing column.

4.3. *Pore pressure*

In order to elaborate on the different behaviors caused by the initial packing of the granular column, the simulated dynamic pore pressure at $x_1 = 11.5$ cm are presented in Fig. 6, where $p_d = p_f - \rho_w g h$. There is a positive pressure inside the granular mass for Case 1 (loose packing), but a negative pressure for Case 2 (dense packing), which are consistent of the experimental observation of Rondon et al. [2011]; the positive/negative pressure is related to the contractancy/dilatancy behavior of the

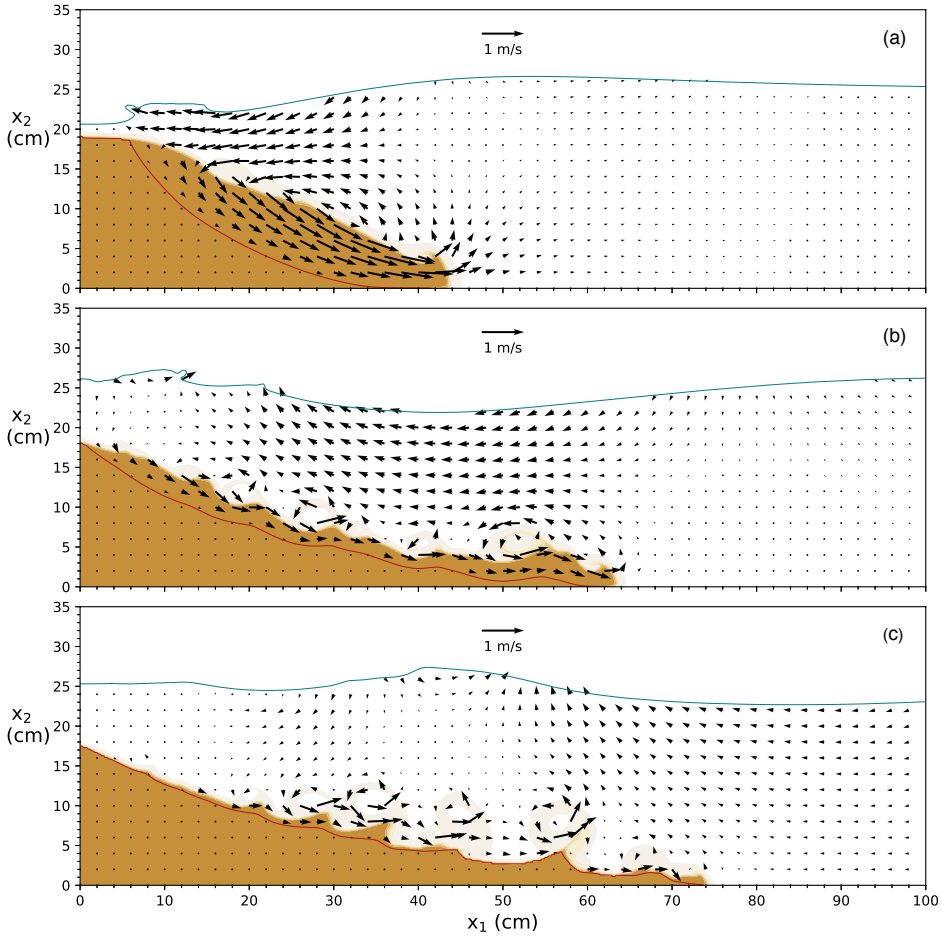

Fig. 4. The computed flow fields at $t = 0.4$ s (a), 0.8 s (b), and 1.2 s (c) for Case 1. The red lines, representing contours for $|\mathbf{u}^s| = 5$ cm/s, are considered to be the failure lines

granular material in motion. The positive/negative pressure can directly generate an outward/inward relative flow between the two phases, indirectly affecting the drag force due to seepage flow [Lee and Huang, 2018] and increasing/decreasing the collapse speed. Previous studies [Abadie et al., 2012; Gauer et al., 2005; Horrillo et al., 2013] considered landslides as a single-phase motion and thus cannot reveal the effect of pore pressure on collapse process.

4.4. *The volume of sliding mass and the volume-averaged sliding velocity*

The landslide volume and its velocity are two important factors determining the strength of a tsunami. Becasue we are studying a two-dimensional problem, the

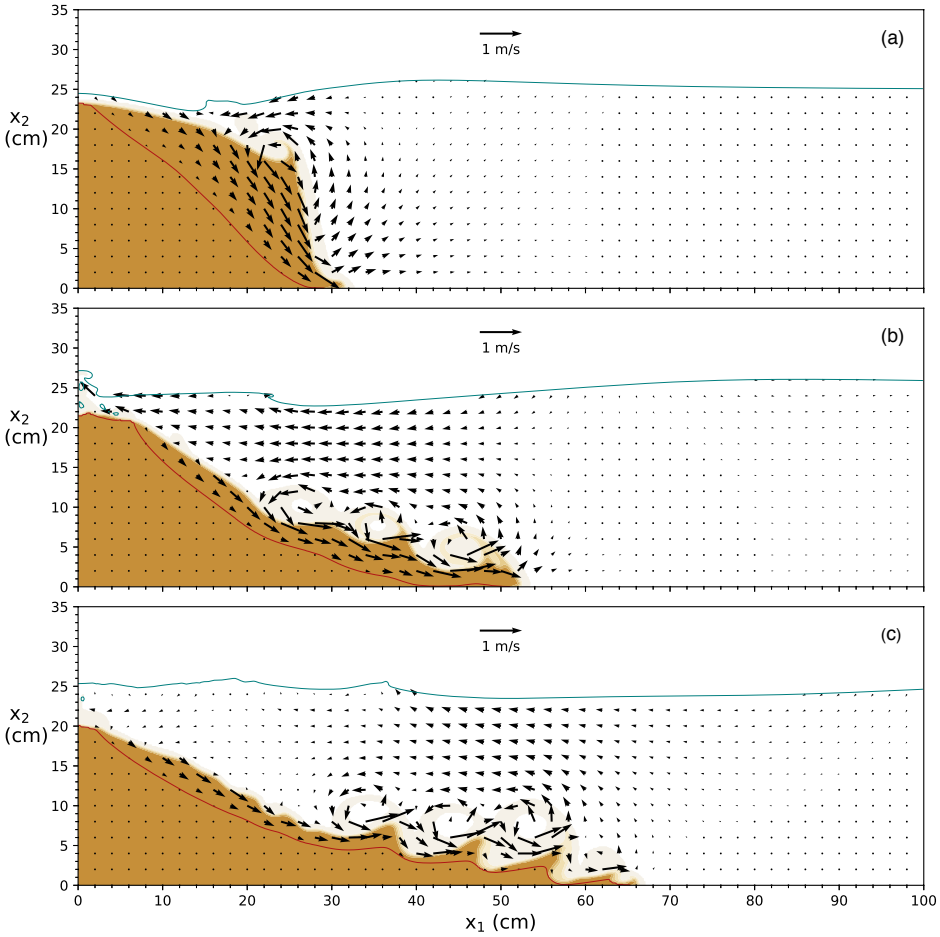

Fig. 5. Snapshots of flow fields at $t = 0.4$ s (a), 0.8 s (b), and 1.2 s (c) for Case 2.

volume of sliding mass can be represented by the area of the sliding mass instead. Both the sliding area and velocity are expected to be time-variant. The area of the sliding mass, SA, (which is actually the volume of the sliding mass since the simulation is two dimensional) are calculated by the following equation:

$$SA = \iint_{\mathbb{A}|_{|\mathbf{u}^s|\geq 5cm/s}} c \quad dx_1 dx_2, \tag{10}$$

where $\mathbb{A}$ is the area of the whole computation domain. The two components of the volume-averaged sliding velocity, u_1 and u_2, are calculated by

$$u_1 = \frac{1}{SA} \iint_{\mathbb{A}|_{|\mathbf{u}^s|\geq 5cm/s}} c u_1^s \quad dx_1 dx_2 \tag{11}$$

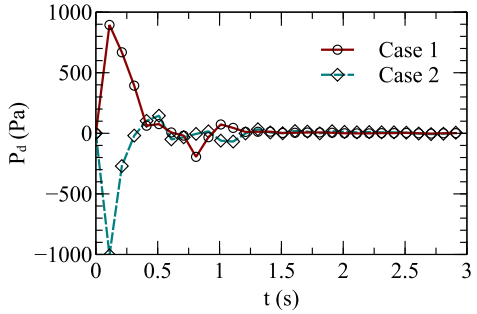

Fig. 6. The time series of the simulated dynamic pore pressure at $x = 11.5$ cm.

and

$$u_2 = \frac{1}{SA} \iint_{\mathbb{A}|_{|\mathbf{u}^s| \geq 5cm/s}} cu_2^s \quad dx_1 dx_2. \tag{12}$$

Fig. 7 shows the simulated sliding areas for the two cases. In the early stage, the sliding area expands very fast. After reaching the maximum, the sliding area begins to decrease gradually, and becomes zero when the collapse process stops. For the initially-loose packing condition, the maximum sliding area is reached at $t = 0.1$ s, and the sliding area drops to about one half of its maximum at $t = 0.4$ s; for the initially-dense packing condition, the maximum sliding area is reached at $t = 0.4$ s, and the sliding area drops to about one half of its maximum at $t = 1.5$ s. The maximum sliding area for the initially-loose packing condition is almost two times larger than that for the initially-dense packing condition.

Fig. 8 shows the two components of the volume-averaged sliding velocity for the two cases. The horizontal velocity reflects the advancing speed of the sliding mass, but the vertical component reflects the descending speed of the sliding mass. Both components are not equal to zero at $t = 3.0$ s because of the suspended sediment, which takes a longer time to settle down. For the initially-loose packing condition, the horizontal velocity reaches its maximum at about $t = 0.5$ s, and then drops to one half of its maximum at about $t = 1.1$ s; for the initially-dense packing condition, the horizontal velocity reaches its maximum at about $t = 0.7$ s, and then drops to one half of its maximum at about $t = 1.7$ s. For both cases, the vertical component is always negative, suggesting a continuous decrease in the potential energy of the granular mass which is associated with the descending of the sliding mass. The volume of the sliding mass descends during the entire collapse process. The maximum descending velocity is found at $t \approx 0.3$ s for Case 1 and $t \approx 0.4$ s for Case 2. Unlike the maximum advancing speed, the maximum descending speed is slightly larger for the initially-dense packing condition. Lee and Huang [2018] simulated the collapses of submerged granular columns, and examined both initially-loose packing and initially-dense packing. They found that the interfacial forces near the top of the column should point downward for the initially-dense packing case

but upward for the initially-loose packing case. This explains why that maximum descending speed is larger for the initially-dense packing condition.

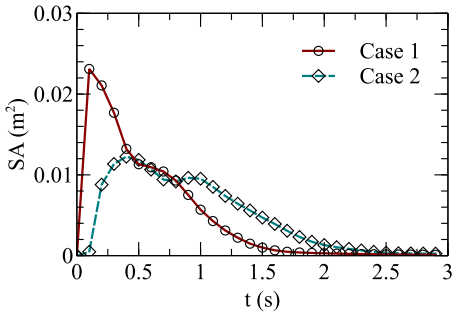

Fig. 7. The computed sliding areas (SA) for Case 1 and Case 2.

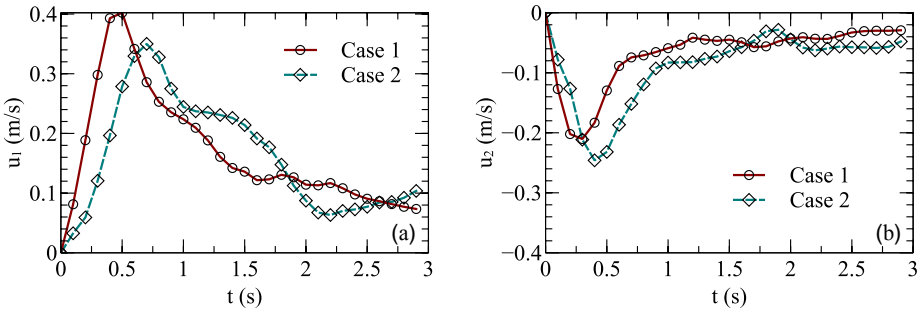

Fig. 8. The mean velocity in (a) the horizontal and (b) the vertical directions for Case 1 and Case 2.

4.5. *The resultant waves recorded at several locations*

Fig. 9 shows the resultant waves recorded by the four virtual wave gauges at locations shown in Fig. 1. The waves recorded by Gauge 1 (whose location coincides with the right edge of the initial column) are led by a wave trough, but the waves recorded by Gauges 2-4 all have a leading positive wave, followed by a larger wave trough. We remark that it has been noticed that tsunamis generated by submarine landslides can be led by a low wave crest followed by a trough up to three times greater in amplitude [Bryant, 2014].

Generally speaking, the resultant waves for an initially-loose parking condition are larger and have an early arrival time at each of the virtual gauges. The relatively larger trough found in the initially-loose packing case is believed to be related to its

rapid collapse process. Strong wave dispersion can be observed in the early stage of the collapse process. Another important point to note is that the period of the resultant waves for the initially-dense packing case is longer due to its slow collapse process.

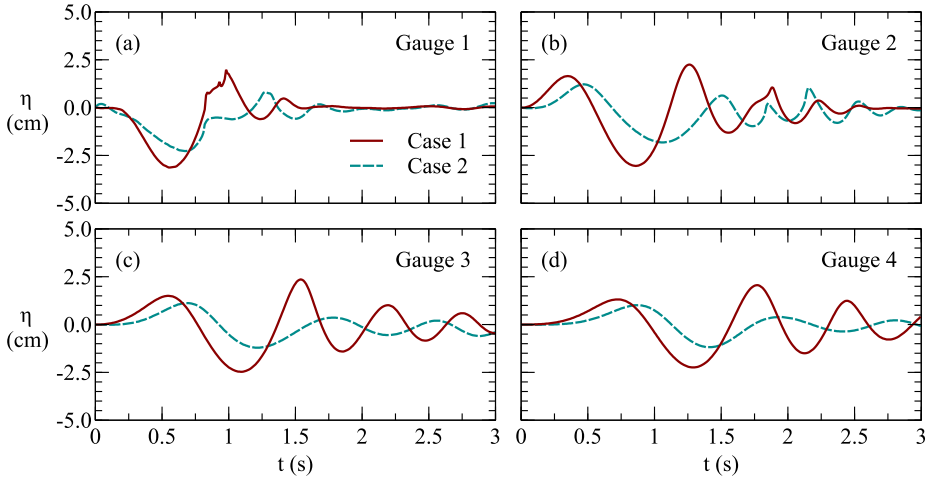

Fig. 9. Time histories of free-surface elevation at different locations for Case 1 and Case 2.

5. Conclusions

This study presented a numerical study of the collapse of a submerged granular column and the resultant surface waves. The numerical simulations were carried out using a three-phase (solid-water-gas) flow model. Numerical results for the collapse of a submerged granular column under two packing conditions were reported: initially-loose packing and initially-dense packing. The following conclusions can be drawn from this numerical study:

(1) The initial packing can greatly influence the duration of the collapse process: the submerged granular column with an initially-loose packing condition collapses faster.
(2) The waves generated by the collapse of submerged granular columns with different packing conditions are similar in wave form but different in magnitude: the initially-loose packing case results in larger impulsive waves.
(3) For both packing conditions, a large-scale vortex generated by the granular flow front can be found. The motion of this large-scale vortex can penetrate into the sliding granular mass and gradually deceases in strength with the elapse of time. This large-scale vortex motion is found to be responsible for the generation of

a secondary wave. A series of near-periodic small-scale vortex are formed in the later stage of the collapse process.

(4) The pore pressure inside the granular mass, which is positive for the initially-loose packing case but negative for the initially-dense packing case, affects the collapse process.

(5) The volume of granular mass in motion is larger for initially-loose packing case. The granular mass in motion advances and descends; however, the advancing speed is larger for the initially-loose packing case whereas the descending speed is larger for the initially-dense packing case.

It is concluded that the initial packing of a submerged granular column can have significant impact on the collapse process and the resultant waves. Therefore, numerical simulations of tsunami generated by submarine landslides need to consider the effects of initial packing of the submerged granular mass.

Acknowledgment

This study is supported partially by the Ministry of Science and Technology, Taiwan (MOST 106-2221-E-032-029) and the US National Science Foundation under grant No. CBET-1706938. Conghao Xu, a PhD candidate of SOEST at the University of Hawaii at Manoa, is acknowledged for this contribution to the code development and verification using the Extreme Science and Engineering Discovery Environment (XSEDE) through a Startup Allocation (OCE170015). Any opinions, findings, and conclusions or recommendations expressed in this material are those of the author(s) and do not necessarily reflect the views of the National Science Foundation. This is SOEST contribution No 10318.

References

Abadie, S. M., Harris, J. C., Grilli, S. T. and Fabre, R. [2012] "Numerical modeling of tsunami waves generated by the flank collapse of the Cumbre Vieja Volcano (La Palma, Canary Islands): Tsunami source and near field effects," *J. Geophys. Res. Ocean.* **117**(5), 1–26.

Assier Rzadkiewicz, S., Mariotti, C, Heinrich, P. [1997] "Numerical simulation of submarine landslides and their hydraulic effects," *J. Waterw. Port Coast. Ocean Eng.*, **123**(4), 149–157.

Boyer, F., Guazzelli, E. and Pouliquen, O. [2011] "Unifying suspension and granular rheology," *Phys. Rev. Lett.* **107**(18), 118301.

Bryant, E. [2014] *Tsunami—The Underrated Hazard 3rd ed.* (Springer and Praxis, UK).

Chatterjee, S., Ghosh, S.,Chatterjee, M. [1994] "Local scour due to submerged horizontal jet," *J. Hydraul. Eng.* **120**, 973-992.

Enet, F. and Grilli, S. T. [2007] "Experimental study of tsunami generation by three-

dimensional rigid underwater landslides," *J. Waterw. Port, Coastal, Ocean Eng.* **133**(6), 442–454.

Engelund [1953] *On the laminar and turbulent flows of ground water through homogeneous sand* (Danish Academy of Technical Sciences, Copenhagen).

Forterre, Y. and Pouliquen, O. [2008] "Flows of dense granular media," *Annu. Rev. Fluid Mech.* **40**, 1–24.

Fritz, H. M., Hager, W. H. and Minor, H. E. [2003] "Landslide generated impulse waves. 2. Hydrodynamic impact craters," *Exp. Fluids* **35**(6), 520–532.

Gauer, P., Kvalstad, T. J., Forsberg, C. F. Bryn, P. and Berg, K. [2005] "The last phase of the Storegga Slide: Simulation of retrogressive slide dynamics and comparison with slide—scar morphology," *Mar. Pet. Geol* **22**(1-2), 171–178.

Grilli, S. T., Shelby, M., Kimmoun, O., Dupont, G., Nicolsky, D., Ma, G., Kirby, J. T., and Shi, F. [2017] "Modeling coastal tsunami hazard from submarine mass failures: effect of slide rheology, experimental validation, and case studies off the US East Coast," *Nat. Hazards* **86**(1), 351–391.

Heinrich, P. [1992] "Nonlinear water waves generated by submarine and aerial landslides," *J. Waterw. Port Coast. Ocean Eng.* **118**(3), 249-266.

Hill, J., Collins, G. S., Avdis, A., Kramer, S. C. and Piggott, M. D. [2014] "How does multiscale modelling and inclusion of realistic palaeobathymetry affect numerical simulation of the Storegga Slide tsunami?," *Ocean Model.* **84**, 11–25.

Hinze, J. [1972] *Turbulence: An Introduction to Its Mechanism and Theory* (McGraw-Hill, New York).

Hirt, C. W. [1981] "Volume of fluid (VOF) method for the dynamics of free boundaries," *J. Comput. Phys.*, **39**(1), 201–225.

Horrillo, J., Wood, A., Kim, G. B. and Parambath, A. [2013] "A simplified 3-D Navier-Stokes numerical model for landslide-tsunami: Application to the Gulf of Mexico," *J. Geophys. Res. Ocean.* **118**(12), 6934–6950.

Hsu, T. J., Jenkins, J. T. and Liu, P. L. F. [2004] "On two-phase sediment transport: sheet flow of massive particles," *Proc. R. Soc. A Math. Phys. Eng. Sci.* **460**(2408), 2223–2250.

Jasak, H. [2009] "OpenFOAM: Open source CFD in research and industry," *Inter. J. Nav. Arch. Oc. Engng.* **1**(2), 89–94.

Lee, C. H., Huang, Z. and Chiew, Y. M. [2015] "A three-dimensional continuum model incorporating static and kinetic effects for granular flows with applications to collapse of a two-dimensional granular column," *Phys. Fluids* **27**, 113303.

Lee, C. H., Low, Y. M. and Chiew, Y. M. [2016] "Multi-dimensional rheology-based two-phase model for sediment transport and applications to sheet flow and pipeline scour," *Phys. Fluids* **28**, 053305.

Lee, C. H and Haung, Z. [2017] "A three-phase flow model and its application to landslide-generated waves," *The 9th South China Sea Tsunami Workshop.*,Qingdao, China, pp. 39.

Lee, C. H and Haung, Z. [2018] "A two-phase flow model for submarine granular

flows: With an application to collapse of deeply-submerged granular columns," *Adv. Water Resour.*, doi:10.1016/j.advwatres.2017.12.012 (In Press).

Lee, C. H., Xu, C. and Huang, Z. [2018] "A three-phase flow simulation of local scour caused by a submerged wall jet with a water-air interface," *Adv. Water Resour.*, doi.org/10.1016/j.advwatres.2017.07.017(In Press).

Liu, P. L. F., Wu, T. R., Raichlen F., Synolakis, C. E. and Borrero, J. C. [2005] "Runup and rundown generated by three-dimensional sliding masses," *J. Fluid Mech.* **536**, 107–144.

Løvholt, F., Pedersen, G., Harbitz, C. B., Glimsdal, S. and Kim, J. [2015] "On the characteristics of landslide tsunamis," *Philos. Trans. R. Soc* **373**, 1–18.

Løvholt, F., Bondevik, S., Laberg, J. S., Kim, J. and Boylan, N. [2017] "Some giant submarine landslides do not produce large tsunamis," *Geophys. Res. Lett.* **44**, 8463–8472.

Ma, G., Kirby, J. T., Hsu, T. J. and Shi, F. [2015] "A two—layer granular landslide model for tsunami wave generation: Theory and computation," *Ocean Model.* **93**, 40–55.

Meruane, C., Tamburrino, A. and Roche, O. [2010] "On the role of the ambient fluid on gravitational granular flow dynamics," *J. Fluid Mech.* **648**, 381–404.

Meruane, C., Tamburrino, A. and Roche, O. [2012] "Dynamics of dense granular flows of small-and-large-grain mixtures in an ambient fluid," *Phys. Rev. E* **86**(2), 026311.

Richardson, J. F. and Zaki, W. N. [1954] "Sedimentation and fluidisation: Part I," *Trans. Instn. Chem. Engrs.* **32**, S82–S100.

Rondon, L., Pouliquen, O. and Aussillous, P. [2011] "Granular collapse in a fluid: role of the initial volume fraction," *Phys. Fluids* **23**(7), 73301.

Shi, C., An, Y., Wu, Q., Liu, Q. and Cao, Z. [2016] "Numerical simulation of landslide-generated waves using a soil-water coupling smoothed particle hydrodynamics model," *Adv. Water Resour.* **92**, 130–141.

Si, P., Aaron, J., McDougall S, Lu, J., Yu, X. Roberts, N. J. and Clague, J. J. [2017] "A non-hydrostatic model for the numerical study of landslide-generated waves," *Landslides*, 1–16. doi: 10.1007/s10346-017-0891-y

Topin, V., Monerie, Y., Perales, F. and Radjaï, F. [2012] "Collapse dynamics and runout of dense granular materials in a fluid," *Phys. Rev. Lett.* **109**(18), 188001.

Trulsson, M. and Andreotti, B. and Claudin, P. [2012] "Transition from the viscous to inertial regime in dense suspensions," *Phys. Rev. Lett.* **109**(11), 118305.

Viroulet, S., Sauret, A., Kimmoun, O. and Kharif, C. [2013] "Granular collapse into water: Toward tsunami landslides," *J. Vis.* **16**(3), 189–191.

Wang, C., Wang, Y., Peng, C. and Meng, X. [2017] "Dilatancy and compaction effects on the submerged granular column collapse," *Phys. Fluids* **29**(10), 103307.

White, F. M. [2000] *Viscous Fluid Flow* (McGraw-Hill, Singapore).

Yavari-Ramshe, S. and Ataie-Ashtiani, B. [2016] "Numerical modeling of subaerial and submarine landslide-generated tsunami waves-recent advances and future

challenges," *Landslides* **13**(6), 1325–1368.